Exploring for Aerodynamic and Structural Design Constraints in the Multi-Objective Rotor Blade Airfoil Optimization Framework

Joon W. Lim
U.S. Army Combat Capabilities Development Command Aviation & Missile Center
Ames Research Center
Moffett Field, California, U.S.A.

Luke D. Allen
U.S. Army Engineer Research and Development Center
Hanover, New Hampshire, U.S.A.

Robert H. Haehnel
U.S. Army Engineer Research and Development Center
Hanover, New Hampshire, U.S.A.

Ian D. Dettwiller
U.S. Army Engineer Research and Development Center
Vicksburg, Mississippi, U.S.A.

ABSTRACT

A rotor blade design optimization framework has been developed by integrating the Dakota, C81Gen, ParFoil, and RCAS software packages in Galaxy. Parameterizing the airfoils using ParFoil was performed prior to the rotor blade optimization. Using Dakota's Multi Objective Genetic Algorithm (MOGA), global design optimization was successfully carried out for the UH-60A rotor blade. It shows a 12.2% reduction at $\mu = 0.4$, a 9.4% reduction at $\mu = 0.35$ and a 3.0% reduction in hover. The expansion of flight envelope is also explored by examining the aerodynamic responses of the optimized rotor under high load conditions. It is found that the optimized rotor designed under the normal cruise condition fails to meet performance expectations when it is exposed to high load conditions where rotor encounters the retreating blade stall. Realistic rotor blade design therefore needs to include a high load condition so that a rotor can perform well at high thrust and high speed.

INTRODUCTION

Rotorcraft, with their capability to take off and land practically anywhere, have demonstrated great versatility for civilian as well as military applications. However, rotorcraft encounter unique challenges compared to fixed-wing aircraft due to widely varying flight conditions at which a main rotor is operated throughout the flight envelope. The improved design of a rotor blade would offer significant advantages to overcome these challenges although it is a difficult task due to the complex nature of aerodynamic and structural environments in the rotorcraft operational envelope.

Rotor blade design optimizations began to draw attention from the rotorcraft community in the 1980s[1]-[3]. During that period, the limited computational resources, combined with the relatively low accuracy of rotor simulations, restrained from conducting large-scale, realistic blade design optimization studies. Since the 2000s, confidence for the accuracy of rotor simulation tools has been significantly improved along with the development of high-fidelity rotorcraft analysis tools[4], and rich computational resources have become available to the designers. Since then, rotor design optimization studies have been more frequently presented.

Leon et al.[5] presented a multi-objective aerodynamic optimization study for an ERATO rotor[6] using the Dakota[6] CONMIN/elsA/HOST computation chain. Design parameters were blade twist, chord and sweep, and as a result the forward flight rotor power at $\mu = 0.344$ was reduced by 1% at best along with the Figure of Merit (FM) improved.

Ortun et al.[7] performed a blade optimization using Dakota CMA-ES/HOST with the design parameters of blade twist and anhedral. A structural design was included in the optimization chain. The design objective was to minimize a main rotor shaft power in forward flight for a European Clean Sky Green Rotorcraft Integrated Technology Demonstrator 5-bladed rotor. As a result, a 3.8% rotor power reduction was achieved at 140 knots (μ=0.36). However, the a posteriori high fidelity prediction using elsA/HOST indicated that Figure of Merit was worsened by 1.8 counts and the maximum blade-vortex-interaction noise increased over 8dB at 65 knots in descending.

Imiela and Wilke[9] presented the rotor blade optimization results for an EC1/EC2 rotor using low-to-high fidelity analysis tools. The design parameters included blade twist, chord, sweep and anhedral. A design optimization was performed

Presented to the 48th European Rotorcraft Forum, Winterthur, Switzerland, September 5-9, 2022.

using the Dakota/METAR/Euler computation chain. The resulting rotor power was reduced by 2.2% at 240 km/h (μ=0.334). Rotor Figure of Merit was worsened by 0.5%, but this is not surprising since hover Figure of Merit was not included in the design objective during the optimization. There are more blade design studies available for rotor performance considerations[10]-[13]. However, the outcomes of all these studies seem distant from a realistic rotor design although they adopted rigorous numerical optimization techniques.

Using an automated Galaxy framework, rotor blade design optimization works have been recently presented[14]-[17]. In these efforts the Galaxy framework is used for optimizing a UH-60A main rotor blade that consists of multiple airfoil sections along the blade span. The framework employed a Multi-Objective Genetic Algorithm[18] along with the airfoil parameterization code ParFoil[19] to morph the airfoil geometries in several blade segments with the objective of minimizing the rotor power in hover and forward flight.

The objective of this study is to better understand deficiencies in the Galaxy framework for a realistic blade design tool, which will be done by examining blade structural and aerodynamic responses in a wider blade design space. Findings will be integrated to the Galaxy framework in terms of design constraints or objective functions in the future.

COMPUTATIONAL METHODOLOGY

Complex digital workflows involving multiple disciplines can impose a tremendous burden on analysts for pre- and post-processing work that include setting up input files, converting data between modules, or generating visual representations of data. For repeated simulations it can be advantageous that the workflow is automated. The automated workflows used in this study are constructed using Galaxy Simulation Builder (GSB)[20] that was developed by Stellar Science, Inc. and the Air Force Research Laboratory.

Galaxy System

Galaxy is a high performance computing (HPC) capable workflow management system. It has native integration with Dakota and provides design optimization tools in a DoD Supercomputing Resource Center (DSRC) HPC environment. Galaxy Simulation Builder (GSB) is a general purpose GUI tool in Galaxy for controlling the environment and the execution of programs remotely on targeted HPC hosts. GSB differentiates itself by its robust integration ability to connect to the DoD HPC network. GSB streamlines the connection and data transfer automatically to these HPC machines, and manages environment setup, job submission, monitoring, and report generation. Managed by the Galaxy coordinator, GSB can submit small simulations on a local workstation and submit large simulations on DoD HPC hosts.

The rotor blade optimization framework has been developed for rotor blade design optimizations by integrating the modules of Dakota, C81Gen, ParFoil[19] and RCAS[21] using GSB. Figure 1a shows a sketch of the complete Galaxy/ ParFoil/ ParBlade/ iVABS blade design framework. ParFoil (**Par**ametric air**Foil)** builds up a parametric airfoil model. ParBlade[22][23] (**Par**ameterized **Blade**) constructs a parametric blade planform model. These two modules are the primary tools used for the aerodynamic design of rotor blades. iVABS[24] is an integrated VABS composite cross-section design tool and offers an inverse structural cross-section design for composite rotor blades. Note that ParBlade and iVABS are not used in this study.

The Galaxy/ParFoil rotor blade optimization framework comprises two simulation workflows – C81 surrogate model builder and rotor blade optimizer. Figure 1b shows the details of the simulation workflows. The first workflow computes C81 table data using C81Gen[25] at the discrete design points for the airfoil sections along the blade and then constructs surrogate models for C81 tables. The second workflow optimizes a helicopter main rotor using Dakota[6] by means of morphing airfoil sections along the blade. At this stage the morphing of airfoil geometries can take place in a number of blade sections, which is determined by the user setup.

Surrogate Airfoil Builder

The surrogate airfoil builder constructs surrogate tables prior to rotor blade optimization. To build the surrogate tables, the design space is populated with several discrete design points sampled in each design parameter axis and at each sampled design point C81Gen generates a C81 table. Thus, the computation time for building surrogate tables depends on the number of sampled points in the design space. In the present study, the design space is populated with five discrete points along each design parameter axis using a regular sampling (or a regular grid for sampling). Therefore, the sample size become $5^4 = 625$ if four design parameters are chosen.

Parametric airfoil model rebuilds an airfoil geometry using design parameters that are often geometric ordinates or mathematical interpolation polynomials[26][27]. ParFoil used in this study morphs a baseline airfoil to the desired airfoil by augmenting or scaling using design parameters. Since the morphing is performed on the baseline geometry,

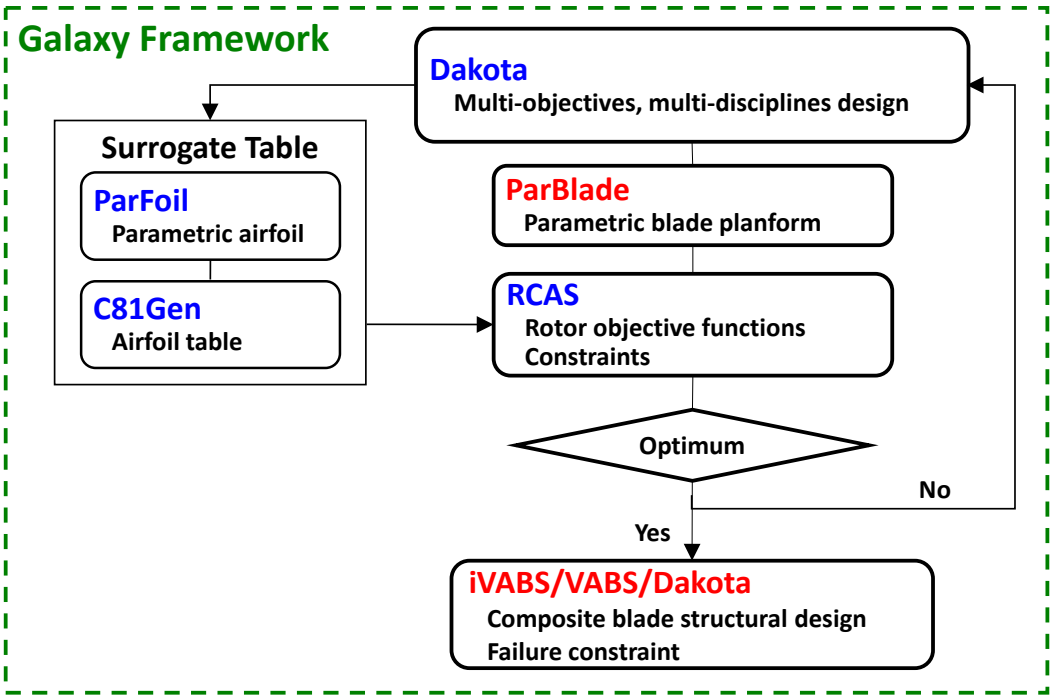

a) Galaxy/ ParFoil/ ParBlade/ iVABS blade design framework

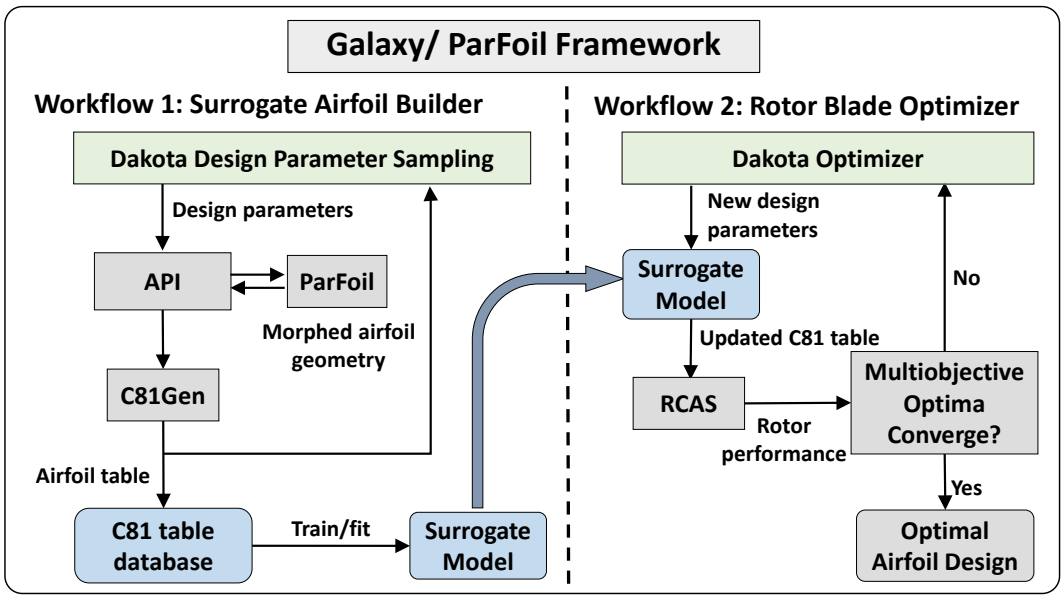

b) The details of Galaxy/ ParFoil simulation workflows

Figure 1. A sketch of the Galaxy-based rotor blade optimization framework comprising Dakota, C81Gen, RCAS, ParFoil, ParBlade and iVABS modules.

some design parameters in the baseline could be kept and so it is not necessary to select all the design parameters for airfoil parametrization.

Design parameters in ParFoil include camber (m), camber crest position (p), thickness (t), thickness crest position (x), leading edge radius (k), trailing edge camber (n), trailing edge camber crest position (q), boat-tail angle (b), and the leading-edge droop (d), as shown in Fig. 2. Prior to the parameterization, airfoil coordinates are redistributed using non-uniform radial basis splines (NURBS)[28]. Then, a desired morphed airfoil section is generated by augmenting delta values to the baseline airfoil geometry or by scaling it.

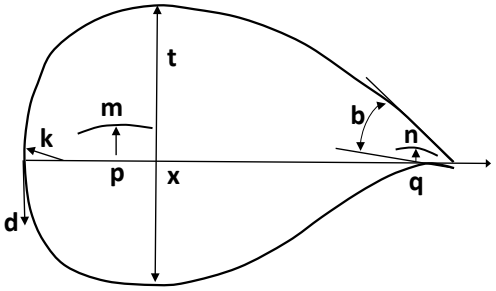

Figure 2. Design parameters in ParFoil.

C81Gen is a GUI wrapper for a 2D airfoil mesh generator and the ARC2D Navier-Stokes solver. ARC2D[29] was developed at the NASA Ames Research Center specifically for airfoil aerodynamics computations and uses an implicit finite difference technique to solve the two-dimensional thin-layer Navier-Stokes equations with a Spalart-Allmaras turbulence model. A fully turbulent option is used for this study.

A C81 surrogate model is constructed by means of multi-dimensional, linear interpolation polynomials between the discrete points, which is capable of computing a new table at any point in the design space. Although a regular sampling is used in this study, it is worth noting that a random or irregular sampling such as Latin hypercube sampling could improve the computational efficiency in design optimizations.

Rotor Blade Optimizer

A simulation workflow has been developed using GSB for rotor blade optimization. In the rotor blade optimizer workflow, a number of modules are executed sequentially to construct C81 tables using the surrogate model and compute RCAS rotor power for the fitness function evaluation.

The rotor blade optimization workflow begins from the user-defined optimization algorithm selected in Dakota (i.e., MOGA). After new design parameter substitution, it then generates new airfoil tables using the surrogate model, replacing expensive CFD calculations within the optimization loop. The next step is to run the RCAS rotorcraft comprehensive module with the newly generated airfoil tables. After the RCAS simulations are complete, the desired performance metrics are extracted and returned to the Dakota optimizer. The iterative optimization process continues by generating new interim populations that contain a batch of design points based on the feasibility metric of the fitness function. Global optimization is complete if the interim populations successfully converge to the Pareto front[15].

ROTOR OPTIMIZATION PROBLEM

An optimal airfoil design for rotor blade is performed using the Galaxy/ParFoil framework. Design parameters are collectively chosen from the ParFoil parameters $\propto_i$ that characterize an airfoil geometry such that

(1) $\alpha_i = \{f_m, \Delta p, f_t, \Delta x, f_k, \Delta n, \Delta q, \Delta b, \Delta d\}_i$

at the i-th blade radial section. Note that *f* indicates a scale factor to the parameter and Δ implies an increment from the baseline value.

In the present study, the design objective is to minimize a rotor power in hover ($C_{p,h}$) and forward flight ($C_{p,f}$ at $\mu = 0.3$). Thus, the optimization problem is defined as:

(2) Minimize: $f_1 = C_{p,f}(\alpha_1, \dots, \alpha_n)$
$f_2 = C_{p,h}(\alpha_1, \dots, \alpha_n)$

Subject to: $\alpha_i \in X_i, \quad i = 1, \dots, n$
$g_i - 1 \leq 0$

where *n* is the number of blade radial locations and X_i is the feasible design space at the i-th radial location. The inequality constraint g_i is defined such that a half peak-to-peak pitch link load at an advance ratio of 0.3 does not exceed the baseline value, which would be given as

(3) $g_i(\alpha_1, \dots, \alpha_n) = \frac{PLL_{half\ pk-pk}}{PLL_{half\ pk-pk,BL}}$

DISCUSSION

A full-scale wind tunnel test of the UH-60A main rotor[30] was performed in the USAF National Full-Scale Aerodynamics Complex (NFAC) 40- by 80-foot wind tunnel at NASA Ames Research Center. The test data measured at the NFAC wind tunnel provides a wealth of information for trim, rotor balance, blade pressure and strain gauge data. The purpose of rotor blade design optimization in this study is to minimize rotor power in hover and forward flight for the UH-60A rotor tested at the NFAC wind tunnel.

Optimized Rotor Performance

The standard UH-60A main rotor has a radius of 322 inches operating at 258 RPM. The standard rotor is made up of two airfoils: the SC1095 airfoil extending from the blade root to 0.48R, the SC1094R8 airfoil from 0.48R to 0.84R, and then returning to the SC1095 from 0.84R to the blade tip.

Design optimization takes place on four distinct blade segments that contain a constant airfoil section. The four segments are the tip segment (Tip: 0.929R to 1.0R), the outboard-1 segment (OB1:

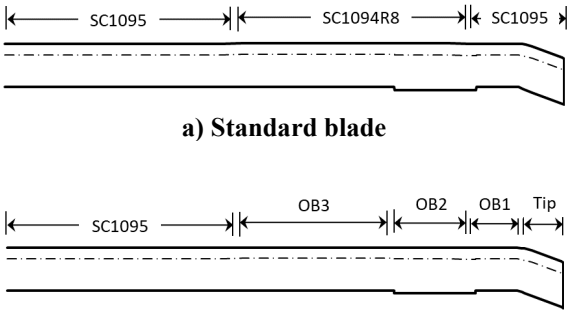

Figure 3. Sketches of the standard UH-60A rotor blade, and the optimized rotor blade with airfoil distributions.

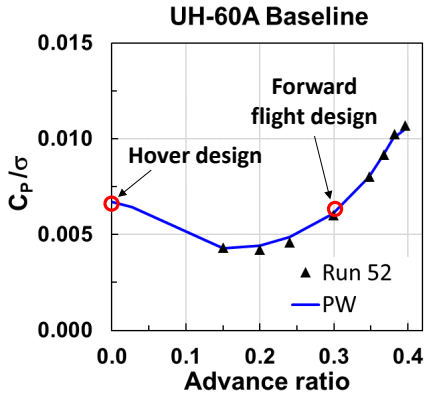

Figure 4. RCAS predictions for the UH-60A baseline rotor performance against NFAC data (C_T/σ = 0.09, σ=0.0826).

0.854R to 0.910R), the outboard-2 segment (OB2: 0.736R to 0.839R) and the outboard-3 segment (OB3: 0.497R to 0.716R). Small gaps between the segments are defined to allow the transition of airfoils smoothly between the segments. Figure 3 shows the sketches of the baseline and optimized blade configurations.

The UH-60A blade model is constructed using the rotorcraft comprehensive code RCAS. The lifting line theory with C81 airfoil tables is used. For the inboard segment having SC1095 (root to 0.48R), experimental values are used for the table. For all outboard segments, C81Gen is used for generating the tables. The differences between the experimental values and the results computed by CFD are not trivial so that failing to use the CFD results could result in an artificially high reduction in rotor power.

The RCAS simulation model uses an isolated rotor with a 4-DOF propulsive trim. Trim targets are thrust, propulsive force, rotor roll and pitch moments. Trim variables are the blade collective,

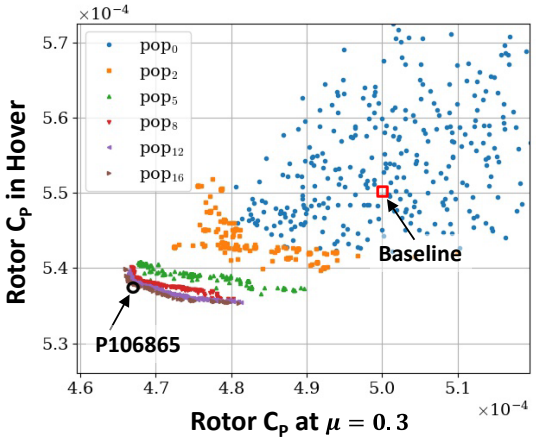

Figure 5. Evolution history of $C_{p,h}$ vs. $C_{p,f}$ for select populations.

lateral and longitudinal cyclic controls and the rotor shaft angle. Figure 4 compares the predicted rotor power coefficients of the UH-60A standard main rotor against the NFAC data (Run 52, C_T/σ = 0.09). The hover and forward flight design points are shown by circles. Prescribed wake (PW) is used in the simulations. The simulation results are aligned well with the NFAC data (Run 52) over a full speed range. It is worth noting that no hover data is available from the NFAC test.

MOGA[18] in Dakota is based on the work of Eddy and Lewis. The algorithm uses distinct-point and clustering metrics to generate a distribution of design points in the Pareto front. Figure 5 illustrates the evolution history of $C_{P,h}$ and $C_{P,f}$ responses for the select population numbers during the MOGA analysis. The plot shows the progression from the relatively wide range of responses in pop_0, moving toward the final set of non-dominated points making up the Pareto front after 16 populations. The Pareto front is comprised of 95 points, all of which appreciably show reduced C_P for both hover and forward flight ($\mu = 0.3$) in comparison to the baseline. All the design points on this Pareto front represent minimum rotor power with different weighted scores between the two flight conditions.

To examine for more details, one design point (P106865) was chosen with a higher weighted score on the forward flight condition. Figure 6 compares the performance of the optimized rotor blade (P106865) with the baseline. Rotor power reduction is seen consistently over a full speed range with the optimized blade design, indicating a 3.0% reduction in hover and a 7.1% reduction at μ=0.30 compared with the baseline. A 12.2% rotor power reduction is also achieved at the highest speed (μ=0.40) tested in the NFAC wind tunnel.

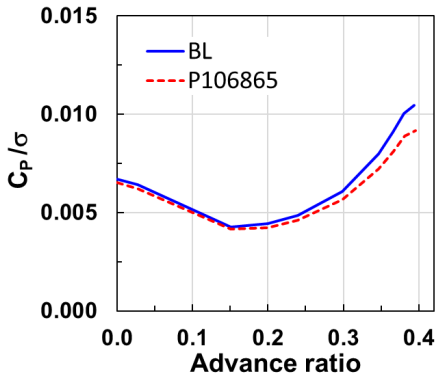

a) Power coefficient

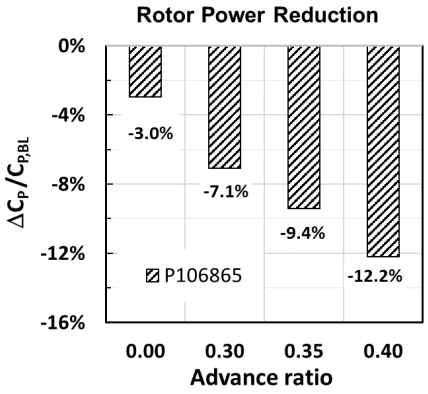

b) Difference in power coefficient

Figure 6. The predicted performance of the UH-60A optimized blade (P106865) over a full range of advance ratios.

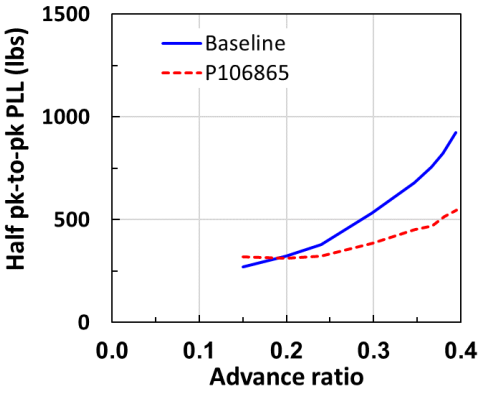

Figure 7. The half peak-to-peak (HP2P) pitch link loads of the optimized blade compared with the baseline.

The optimization problem was set with the pitch link load constraint of limiting a half peak-to-peak (HP2P) pitch link load (PLL) not exceeding the baseline value at the design speed of μ=0.30. Figure 7 compares the half peak-to-peak pitch link load between the baseline and optimized blades over a full speed range. The HP2P pitch link load of the optimized blade is well below the baseline value at the design speed.

Optimal Rotor Blade Design

A blade design optimization was performed for the sections from 0.497R to the tip. Four design parameters (m, p, t, x) were used at the tip or OB1 segment (SC1095) and five design parameters (m, p, t, x, d) were at the OB2 or OB3 segment (SC1094R8). Table 1 describes the ParFoil design parameters and their augmentation strategies for both SC1095 and SC1094R8 airfoils. Table 2 provides the optimal solution at the design point P106865 in Table 2.

Figure 8 compares the optimal airfoil geometries of P106865 with the baseline geometries. The tip and OB1 optimal geometries are compared with the SC1095 in Figure 8a. The OB2 and OB3 optimal geometries are compared with the SC1094R8 in Figure 8b. The figure indicates that the optimal airfoils tend consistently thinner along the blade span compared to the baseline.

Table 1. ParFoil design parameters and augmentation strategies. A zero subscript denotes the baseline value. All the values are given in airfoil chords except the scaling factors, f_m and f_t.

	SC1095	SC1094R8	Strategy	Feasible Bounds
m_0	0.0081	0.0210	$m = m_0 f_m$	$0.0 \le f_m \le 1.5$
p_0	0.2700	0.2124	$p = p_0 + \Delta p$	$-0.0965 \le \Delta p \le 0.1035$
t_0	0.0949	0.0940	$t = t_0 f_t$	$0.5 \le f_t \le 1.3$
x_0	0.2700	0.2733	$x = x_0 + \Delta x$	$-0.1 \le \Delta x \le 0.25$
d_0	0.0	-0.0020	$d = \Delta d$	$-0.0030 \le \Delta d \le 0.0$

Table 2. Optimal design parameters (P106865) against the baseline airfoils (SC1095 and SC1094R8). The values are given in airfoil chords.

	SC1095 family			SC1094R8 family		
	Baseline	**Tip**	**OB1**	**Baseline**	**OB2**	**OB3**
m	0.0081	0.0142	0.0100	0.0210	0.0111	0.0030
p	0.2700	0.1748	0.1996	0.2124	0.2692	0.2731
t	0.0949	0.0722	0.0718	0.0940	0.0715	0.0743
x	0.2700	0.3480	0.3148	0.2733	0.2100	0.1845
d	n/a	n/a	n/a	-0.0020	-0.0032	-0.0026

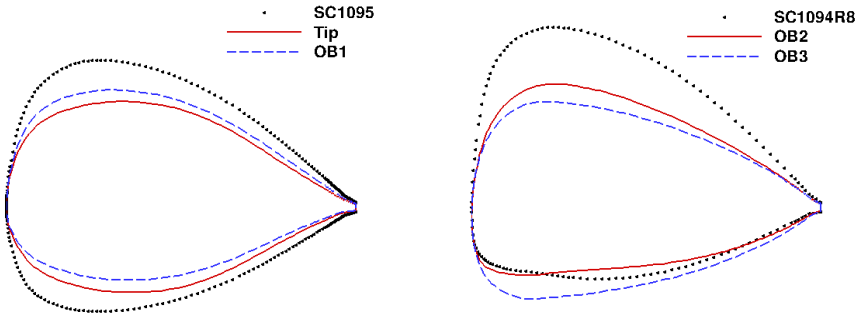

a) SC1095 optimal airfoils **b) SC1094R8 optimal airfoils**

Figure 8. The airfoil geometries of the optimized blade (P106865) at the four segments (Tip, OB1, OB2, OB3) along the blade span compared with the baseline airfoil geometries (not to scale).

Based on the optimal airfoil geometries, C81 tables were generated using the C81Gen tool. Airfoil properties were then derived using the C81 tables. Figure 9 compares the properties of the optimal airfoils with the baseline for the blade tip region (Top, OB1) as well as the outboard region (OB2, OB3). The drag divergence Mach number (M_{dd}) is computed by $\frac{\partial c_d}{\partial M} = 0.1$ with a backward finite difference scheme. The optimal airfoils consistently display higher $c_{l,max}$ at high Mach numbers although they are lower at moderate or low Mach numbers (e.g., M=0.5 and lower) compared with the baseline. The drag divergence Mach numbers of the optimal airfoils are significantly improved. The c_{d0} of the optimal airfoils are lower over a full range of Mach numbers. The c_d of the optimal airfoils is also significantly lower at M=0.8, but it becomes higher at M=0.4 for the relatively larger angles of attack. This implies that the optimal airfoils may be vulnerable to dynamic stall on the retreating side although they are well designed to reduce drag on the advancing side.

Figure 10 compares the sectional lift, drag, and pitching moment coefficients between the baseline and optimized (P106865) blades at $\mu = 0.3$. The contour in the right-hand column shows the difference in the sectional aerodynamic coefficients between the baseline and optimized blades. The tip circular band (between the tip and the long-dashed line) consists of the SC1095 family (Tip, OB1) and the outboard circular band (between the long- and short-dashed lines) consists of the SC1094R8 family (OB2, OB3). The inboard circular band (inside the short-dashed line) consists of the baseline SC1095 airfoil.

Significant improvements for rotor performance are seen on the advancing side with the optimized blade (P106865). The optimal airfoils tend to provide more lift and less drag on the advancing side, whereas they allow slightly more drag on the retreating side. The negative peak of pitching moment on the advancing side is much smaller with the optimal airfoils. It appears that the reduction in rotor power with the optimal airfoils results from a drag reduction and a lift increase on the advancing side.

Rotor Dynamics and Stability

By morphing the airfoil geometries along the blade, a sizable gain was obtained for rotor performance (see Fig. 6). The next step is to find out whether this

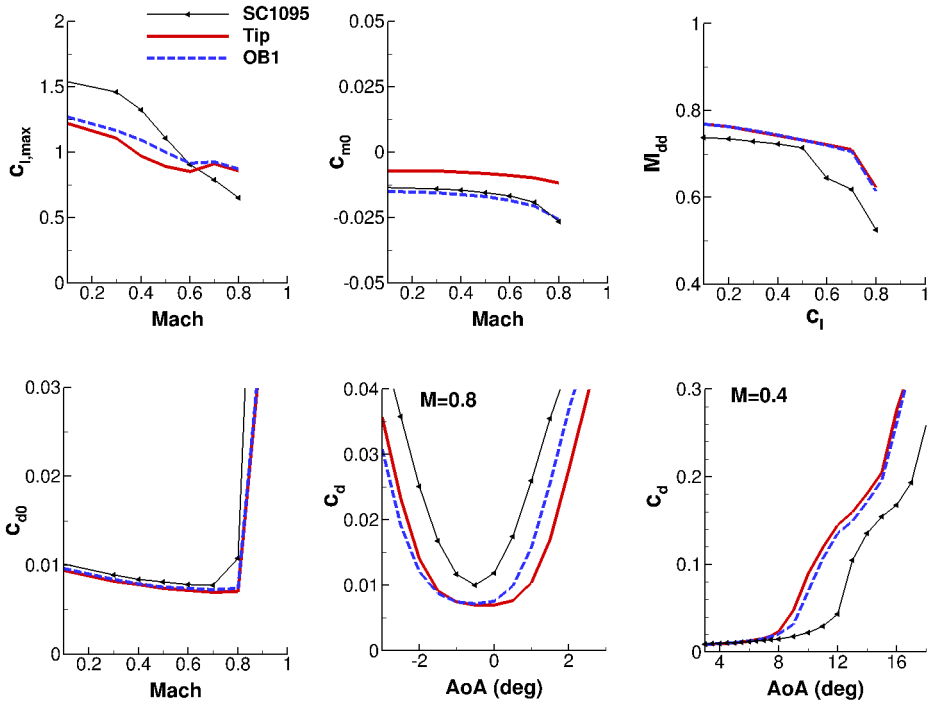

a) SC1095 and its optimal airfoils (tip region)

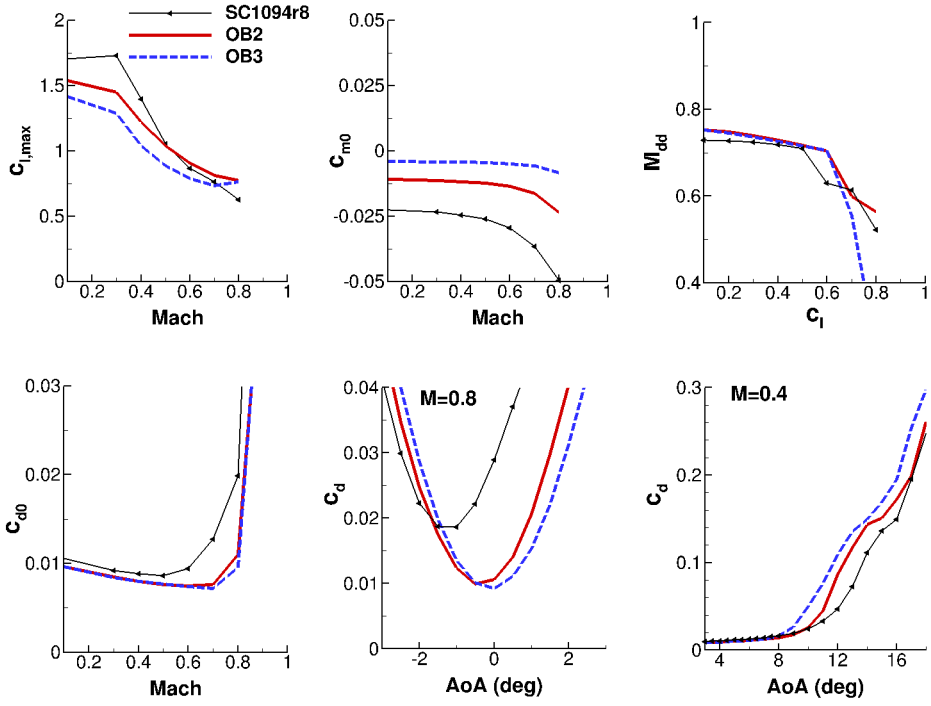

b) SC1094R8 and its optimal airfoils (outboard region)

Figure 9. The UH-60A optimal airfoil properties of the optimized blade (P106865), derived from the C81 tables computed using C81Gen.

gain can adversely influence rotor responses such as blade bending stresses, rotor vibrations, blade instability or rotor noise. Any unfavorable rotor response needs to be limited in the optimization process via design constraints. Figure 11 compares the three components of blade bending moments at

$\mu = 0.3$. M_x is the torsional moment (positive nose up), M_y is the flap moment (positive flap down), and M_z is the lead-lag moment (positive towards the leading edge). Note that the delta difference of moments between the optimized blade and baseline in the contour is based on the absolute value of moment. With thinner airfoils and no blade planform change in the optimized blade airfoils (P106865), any sharp increase in bending moments is not expected. In fact, the bending moments of the optimized blade are mostly lower than the baseline over a full rotor disk.

Rotor vibration is measured using the n-per-rev and 2n-per-rev components of the transferred hub forces and moments in the hub frame for the n-bladed rotor. For example, the 4- and 8-per-rev components are used for the four-bladed rotor. The vibration index is thus defined with the weighting factors that are based on the vibration intrusion index[22] as:

$$(4)\quad VI = \sum_{i=nP,2nP} \left(K_F \frac{F_{H,i}}{W_0} + K_M \frac{M_{H,i}}{RW_0} \right)$$

where

$$F_{H,i} = \sqrt{(0.5F_{xH,i})^2 + (0.67F_{yH,i})^2 + (F_{zH,i})^2}$$

$$M_{H,i} = \sqrt{M_{xH,i}^2 + M_{yH,i}^2}$$

F_H and M_H are the non-rotating hub forces and moments in the hub-fixed coordinate system, W_0 is nominal aircraft weight, and R is blade radius. In this study, W_0 is set 18,000 lbs, R is 322 inches, and K_F and K_M are set to unity.

Figure 12 compares the vibration index between the baseline and optimized blades over a full range of speeds. Slightly lower vibrations are observed with the optimized blade at an advance ratio of 0.2 and higher.

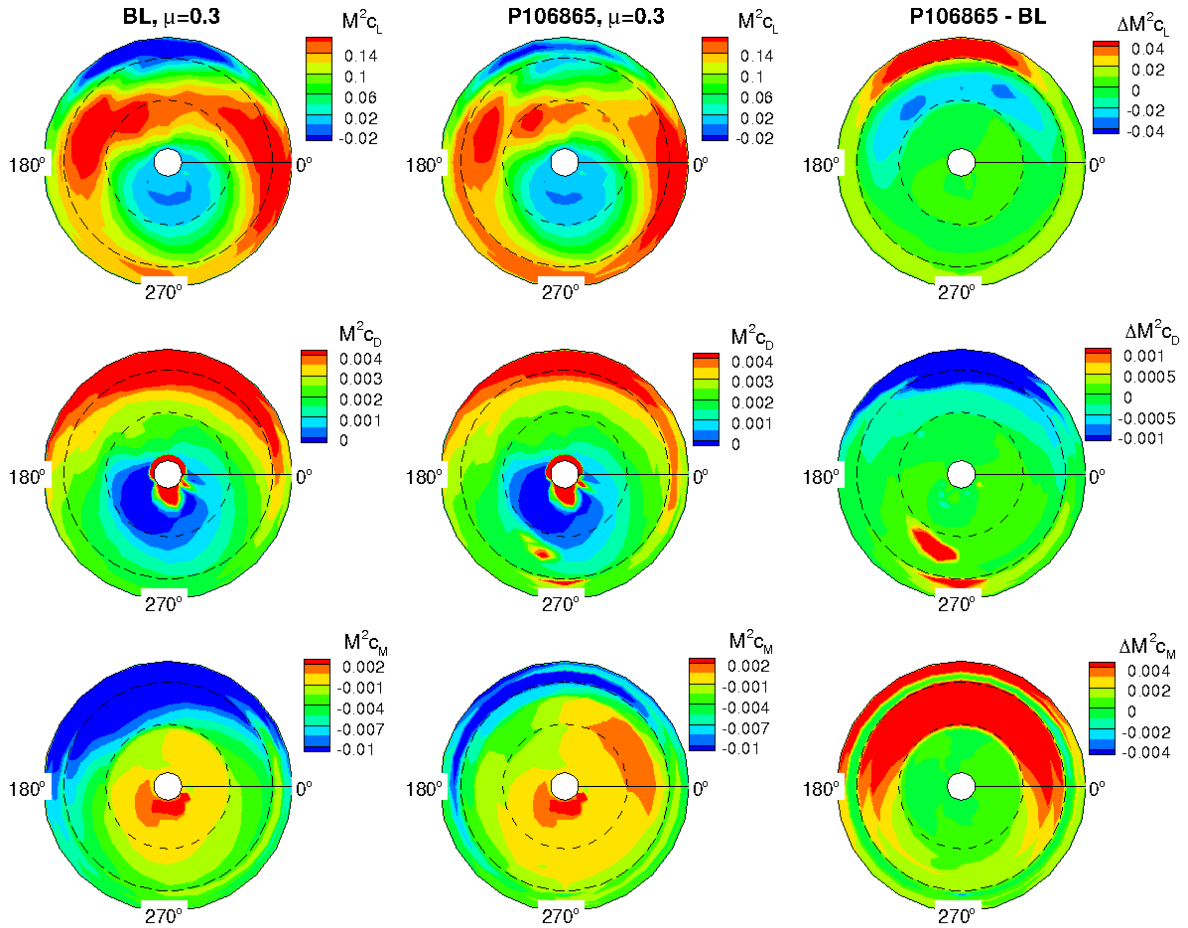

a) Baseline **b) P106865** **c) Difference**

Figure 10. Comparison of the blade lift, drag and pitching moment distributions at $\mu = 0.3$ ($C_T/\sigma = 0.09$, $\sigma = 0.0826$) between the baseline and optimized blades (P106865). The long-dashed circle (r/R=0.84) indicates the inboard end of the SC1095 airfoil family, and the dashed circle (r/R=0.50) indicates the inboard end of the SC1094R8 airfoil family.

Blade stability is also examined in Fig. 13. The critical damping ratio of blade is compared between the baseline (solid line) and the optimized blade (dashed line) for the first few modes including the lead-lag mode (L1), the two flap modes (F1, F2) and the torsion mode (T1). Small differences in critical

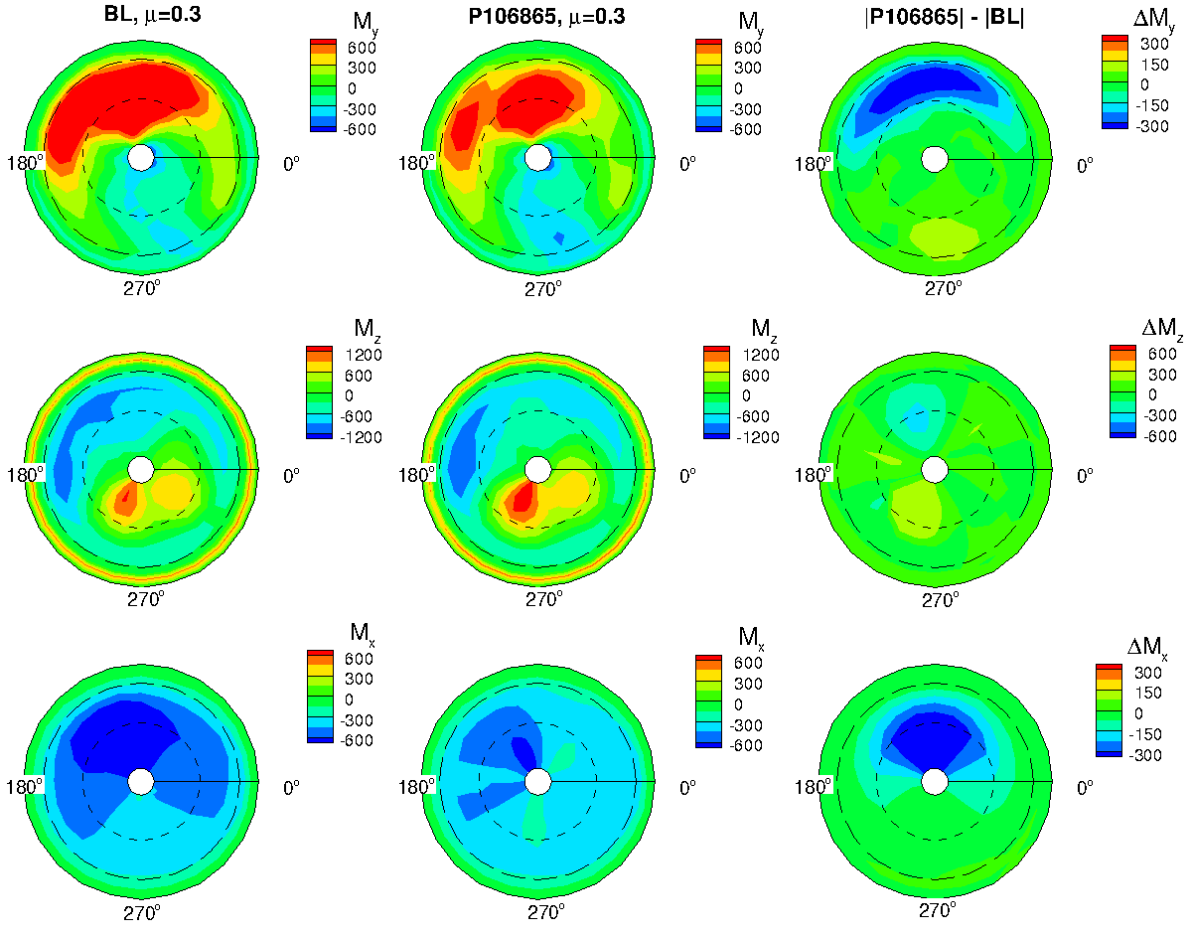

a) Baseline **b) P106865** **c) Difference**

Figure 11. Comparison of the blade moment distributions at μ = 0.3 ($C_T/\sigma = 0.09$, $\sigma = 0.0826$) between the baseline and optimized blades (P106865). Torsional moment is M_x, flap moment is M_y and lead-lag moment is M_z. The long-dashed circle (r/R=0.84) indicates the inboard end of the SC1095 airfoil family, and the dashed circle (r/R=0.50) indicates the inboard end of the SC1094R8 airfoil family.

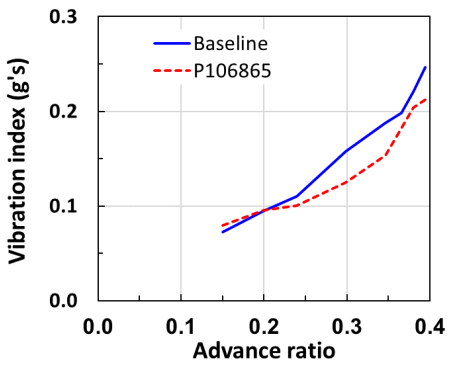

Figure 12. The vibration index of the optimized blade (P106865) compared to the baseline.

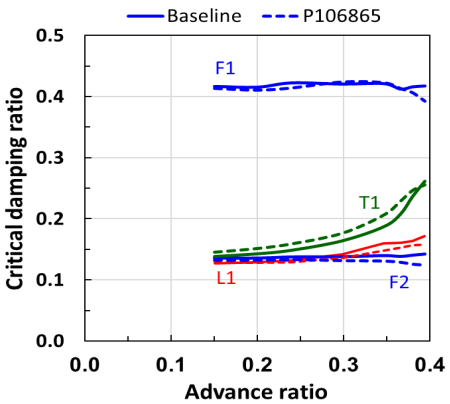

Figure 13. The critical damping ratio of the optimized blade (P106865; dashed line) compared to the baseline (solid line).

damping ratio are observed between the baseline and optimized blades.

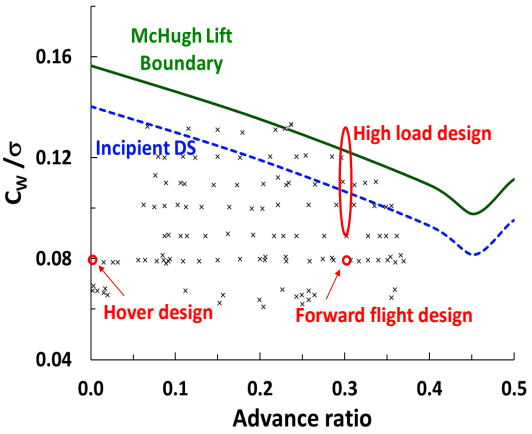

Figure 14. The flight envelope of UH-60A Airloads Program with the McHugh lift boundary and an incipient dynamic stall boundary.

Flight Envelope Expansion

In the high-speed regime, rotor lift is limited largely by blade stall on the retreating side. This rotor lift limit is used to define the boundary of flight envelope. As shown in Fig. 14, Bousman presented the flight envelope for a UH-60A rotor using the UH-60A Airloads Program data, accompanied with the McHugh lift and incipient dynamic stall boundaries[31]. He found that the UH-60A lift boundary was almost identical to the McHugh boundary at an advance ratio of 0.3. It is worth noting that the McHugh lift boundary was derived from the wind tunnel test data of the CH-47B three-bladed, 1/10-th scale rotor[32].

A significant improvement for rotor performance was shown in hover and forward flight with the optimized rotor (see Fig. 6). Now, this optimized rotor will be examined under a high load condition. In this study, the high load condition is determined by incrementally increasing a rotor collective from the trimmed condition at an advance ratio of 0.30 until a rotor lift reversal is found, which is indicated as 'high load design' in Fig. 14.

Figure 15 compares rotor lift and drag between the baseline and optimized rotors (P106865) under the high load condition at an advance ratio of 0.30. The data point, P5231, shown in the figure represents the UH-60A NFAC wind tunnel test data in a trimmed condition at an advance ratio of 0.30 (C_L/σ =0.090, C_P/σ =0.0060, 10.0° rotor collective). The RCAS simulation results are generated by increasing a rotor collective. The rotor collectives in the simulation

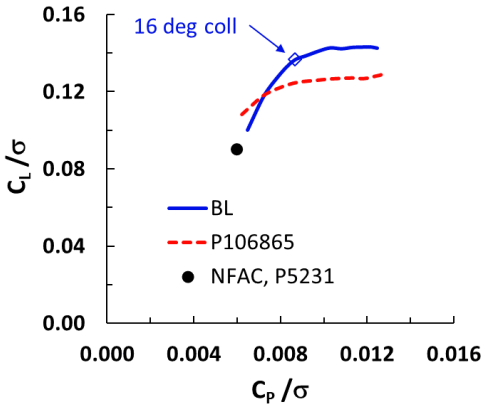

a) Rotor lift coeffcient/solidity

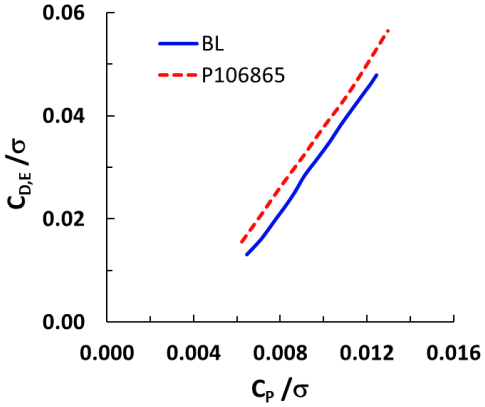

b) Rotor drag coefficient/solidity

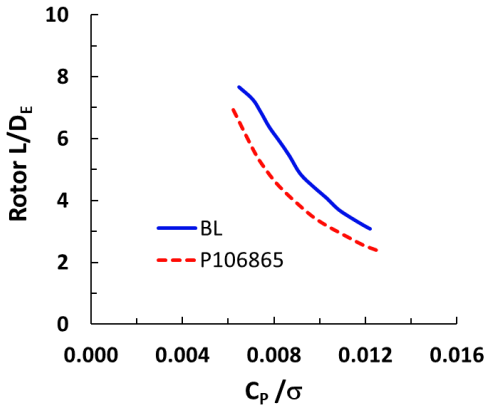

c) Rotor L/D_E/solidity

Figure 15. Comparison of the UH-60A rotor lift, drag and L/D_E between the baseline and the optimized blade (P106865) under the high load condition at an advance ratio of 0.30 and a 16-degree rotor collective (C_T/σ ≈0.13). The geometric solidity σ of UH-60A is 0.0826.

Table 3. The predicted rotor thrust and power coefficients of the baseline and optimized rotors (P106865) at the high load condition at μ = 0.3 and a 16-degree rotor collective (σ = 0.0826).

	Baseline	Optimized	Relative change
C_T/σ	0.1365	0.1252	-0.083
C_P/σ	0.00867	0.00912	0.052
$C_{D,E}/\sigma$	0.02505	0.03262	0.300
L/D_E	5.448	3.838	-0.295

range from 13.0 to 19.4 degrees, which is much higher than the measured 10.0-degree collective at P5231. The 16-degree collective is marked in Fig. 15a, at which further examination will be made for the optimized rotor.

The optimized rotor lift coefficient (C_L/σ) is significantly lower than the baseline when rotor power coefficient (C_P/σ) is high. The optimized rotor equivalent drag ($C_{D,E}/\sigma$) is higher than the baseline. Note that the rotor equivalent drag is calculated using $D_E = (P_i+P_o)/V$ where P_i is an induced power and P_o is a profile power. With its lower rotor lift and higher rotor equivalent drag, the optimized rotor L/D_E becomes lower than the baseline. The RCAS results of rotor thrust and power coefficients at μ = 0.3 and a 16-degree rotor collective are provided in Table3.

Figure 16 compares the contours of aerodynamic responses between the baseline and optimized rotors under the high load condition. Since the optimized

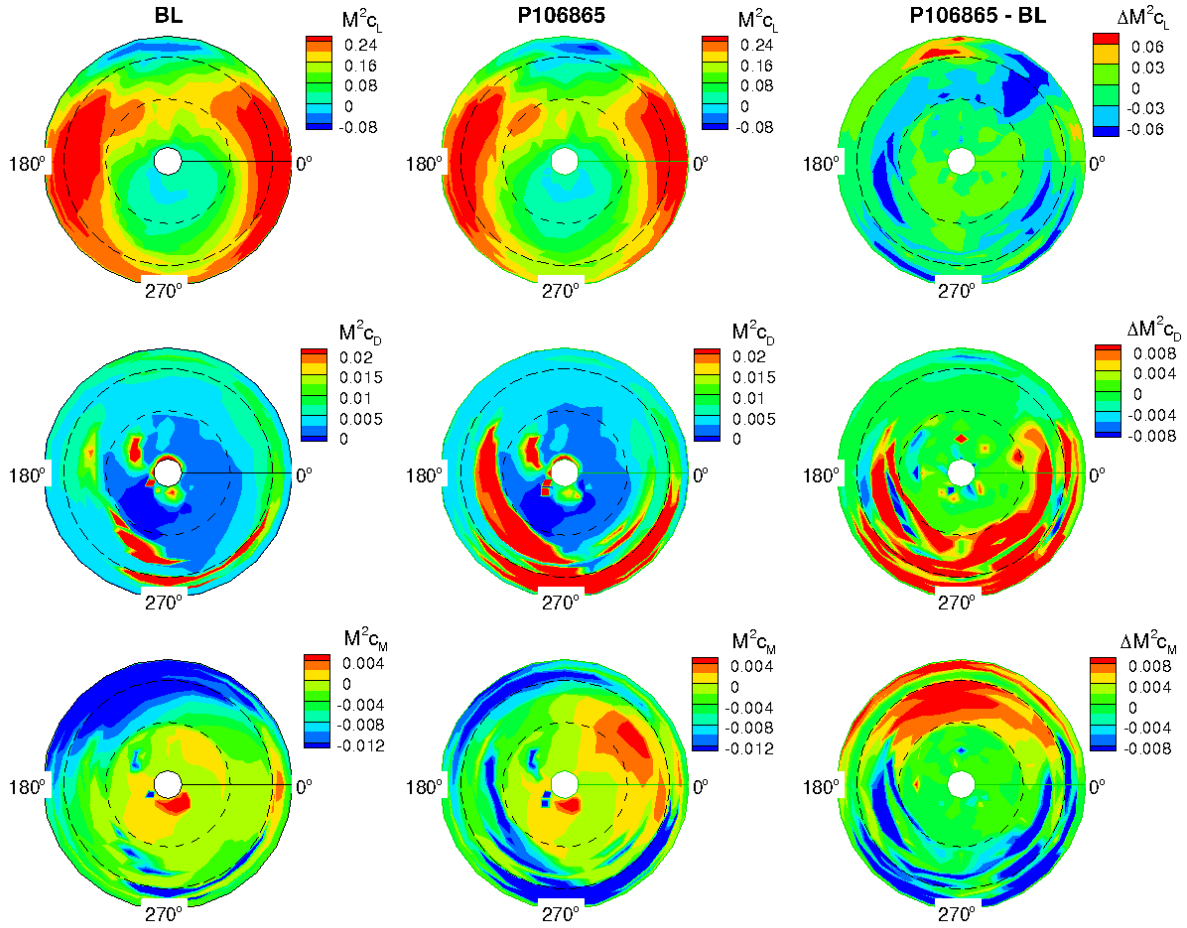

a) Baseline **b) P106865** **c) Difference**

Figure 16. Comparison of the blade lift, drag and pitching moment distributions between the baseline and optimized blades (P106865) under the high load condition at μ = 0.3 and a 16-degree rotor collective ($C_T/\sigma \approx 0.13$). The long-dashed circle (r/R=0.84) indicates the inboard end of the SC1095 airfoil family, and the dashed circle (r/R=0.50) indicates the inboard end of the SC1094R8 airfoil family.

rotor consists of thinner airfoils, it generates lift slightly lower than the baseline in most of the rotor disk. In addition, it generates significantly higher drag on the retreating side than the baseline, which may be linked with the higher drag observed from the optimal airfoil at M=0.4 (refer to Fig. 9). It is obvious that the optimal airfoils are vulnerable to dynamic stall. Although the prescribed wake analysis in RCAS may not be as accurate as a high-fidelity CFD analysis in predicting the onset of stall, it is assumed that the delta differences in aerodynamic responses of the optimized rotor relative to the baseline are reasonably accurate.

Figure 17 compares the sectional aerodynamic responses at r/R=0.675 and 0.775 under the same high load condition. Due to its magnitude on the retreating side, the angle of attack (AoA) seems in the deep stall regime. The c_M is computed by dividing M^2c_M by M^2 and indicates strong dynamic stall on the retreating side although its negative

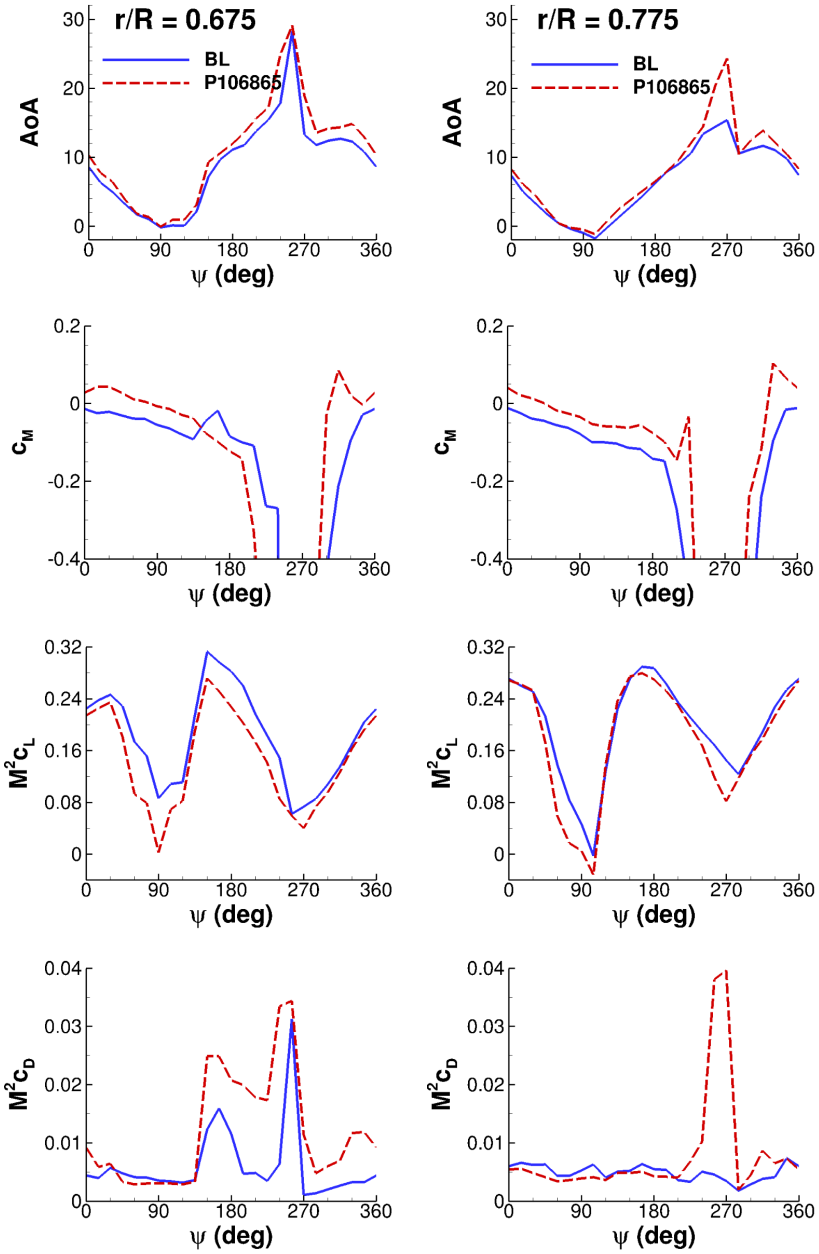

a) r/R = 0.675 b) r/R = 0.775

Figure 17. Comparison of the angles of attack, moment coefficient, sectional rotor lift and sectional rotor drag between the baseline and the optimized blade (P106865) under the high load condition at μ = 0.3 and a 16-degree rotor collective ($C_T/\sigma \approx 0.13$).

down peak is apparently exaggerated. Rotor drag also indicates strong dynamic stall on the retreating side.

Performance and Flight Envelope Combined

Figure 6 demonstrated that rotor performance is significantly improved with the optimized rotor (P106865). The associated optimal design is found mainly with thinner airfoils along the blade span, resulting in a significant reduction in rotor drag on the advancing side. However, this optimized rotor does not behave well under high load conditions because its thinner optimal airfoils induce a higher drag than the baseline airfoils when they encounter deep dynamic stall.

The blade design optimization objective is to minimize rotor power in hover and forward flight, and the high load condition is not considered for a design objective or constraint. Therefore, it is not unexpected that the present optimal rotor design performs poorly under high load conditions. It seems necessary that the high load condition is included in the design optimization if a realistic blade design is desired.

The high load condition is not typically considered in the rotor performance design studies and so there are available few relevant publications. Hansford claimed that the Lynx aircraft with the BERP III rotor was flown at the high thrust condition representing a 39% increase over the standard flight envelope[33][34], which resulted from the change in the blade tip shape as well as airfoils. Two decades later, Harrison et al. reported that the AW101 aircraft with the BERP IV rotor achieved a 5% power reduction in hover, a 10-15% power reduction in cruise and the blade stall envelope improved at least by 10 knots over the AW101 BERP III rotor[35]. The improvements for rotor power and flight envelope expansion were made by changing the blade tip shape and airfoils and also by taking advantage of aeroelastic tailoring for blade structure. The recent presentation made by Min et al. introduced their high speed, highly efficient rotor design (HSHER) with the consideration of hover FM as well as high speed L/D_E[36]. Their best design achieved the FM improvement by 3 counts and the speed enhancement by 30knots. Thus, these studies indicate that feasible rotor blade designs exist for the minimum hover/cruise performance as well as the expansion of flight envelope.

CONCLUSIONS

A rotor blade design optimization framework has been developed by integrating the Dakota, C81Gen, ParFoil, and RCAS software packages in Galaxy. Parameterizing the airfoils using ParFoil was performed prior to the rotor blade optimization. Using Dakota's Multi Objective Genetic Algorithm (MOGA), global design optimization was successfully carried out for the UH-60A rotor blade. The following are key findings from the present study:

1) The design optimization objective was to minimize rotor power at an advance ratio of 0.3 as well as in hover. The optimal blade design showed favorable rotor power reductions over a full range of flight speeds. It showed a 12.2% reduction at $\mu = 0.4$, a 9.4% reduction at $\mu = 0.35$ and a 3.0% reduction in hover. Potential candidates for the design constraint were examined including blade bending moments, rotor vibration and blade damping, but none of them revealed risks for the blade airfoil design optimization.
2) The expansion of flight envelope was explored by examining the aerodynamic responses of the optimized rotor under high load conditions. It was found that the optimized rotor designed under the normal cruise condition failed to meet performance expectations when it was exposed to the high load conditions where rotor encountered the retreating blade stall. Realistic rotor blade design therefore needs to include a high load condition so that a rotor can perform well at high thrust and high speed.

ACKNOWLEDGMENTS

This work was made possible by the HPC Modernization Program's allocation of compute time on the ERDC DSRC's Cray XC40, Onyx.

REFERENCES

[1] Walsh, J. L, Bingham, G. J. and Riley, M. F., "Optimization Methods Applied to the Aerodynamic Design of Helicopter Rotor Blades," *Journal of American Helicopter Society*, Vol. 32, No. 4, 1987, pp. 39-44.

[2] Celi, R. and Friedmann, P. P., "Structural Optimization with Aeroelastic Constraints of Rotor Blades with Straight and Swept Tips," *AIAA Journal*, Vol. 28, Issue 5, May 1990, pp.928-936.

[3] Lim, J. W. and Chopra, I., "Aeroelastic Optimization of a Helicopter Rotor," *Journal of American Helicopter Society*, Vol. 34, No. 1, 1989, pp. 52-62.

[4] Lim, J. W., Nygaard, T. A., Strawn, R., Potsdam, M., "Blade-Vortex Interaction Airloads Prediction Using Coupled Computational Fluid and Structural Dynamics," *Journal of the American Helicopter Society*,

Volume 52, Number 4, 1 October 2007, pp. 318-328.

[5] Leon, E. R., Le Pape, A., Desideri, J., Alfano, D. and Costes, M., "Concurrent Aerodynamic Optimization of Rotor Blades Using a Nash Game Method," American Helicopter Society 69th Annual Forum Proceedings, Phoenix, Arizona, May 21–23, 2013.

[6] Prieur, J. and Splettstoesser, W. R., "ERATO – An ONERA-DLR Cooperative Programme on Aeroacoustic Rotor Optimization," 25th European Rotorcraft Forum Proceedings, Rome, Italy, September 1999.

[7] Adams, B. M., Bohnhoff, W. J., Dalbey, K. R., Ebeida, M. S., Eddy, J. P., Eldred, M. S., Gararci, G., Hooper, R. W., Hough, P. D., Hu, K. T., Jakeman, J. D., Khalil, M., Maupin, K. A., Monschke, J. A., Ridgway, E. M., Rushdi, A. A., Stephens, J. A., Swiler, L. P., Vigil, D. M., Wildey, T. M., and Winokur, J. G., "Dakota, a Multilevel Parallel Object-Oriented Framework for Design Optimization, Parameter Estimation, Uncertainty Quantification, and Sensitivity Analysis: Version 6.11 Users Manual" Sandia National Laboratories SAND2014-4633, 2018. Available: http://dakota.sandia.gov/documentation.html.

[8] Ortun, B., Bailly, J., Mercier des Rochettes, H. and Delrieux, Y., "Recent Advances in Rotor Aerodynamic Optimization, Including Structural Data Update," Fifth Decennial AHS Aeromechanics Specialists' Conference Proceedings, San Francisco, CA, January 22-24, 2014.

[9] Imiela, M and Wilke, G., "Passive Blade Optimization and Evaluation in Off-Design Conditions," 39th European Rotorcraft Forum Proceedings, Moscow, Russia, September 2013.

[10] Johnson, C. and Barakos, G., "Optimisation of Aspects of Helicopter Rotor Blades and Fuselage," 37th European Rotorcraft Forum Proceedings, Gallarate, Italy, September 2011.

[11] Leusink, D., Alfano, D. and Cinnella, P., "Aerodynamic rotor blade optimization at Eurocopter - a new way of industrial rotor blade design," 51st AIAA Aerospace Sciences Meeting Proceedings, Grapevine, Texas, January 2013.

[12] Mavriplis, D., Fabiano, E. and Anderson, E., "Recent Advances in High-Fidelity Multidisciplinary Adjoint-Based Optimization with the NSU3D Flow Solver Framework," 51st AIAA Aerospace Sciences Meeting Proceedings, Grapevine, Texas, January 2013.

[13] Wang, L., Diskin, B., Biedron, R. T., Nielsen, E. J., Sonneville, V. and Bauchau, O. A., "High-Fidelity Multidisciplinary Sensitivity Analysis Framework for Multipoint Rotorcraft Optimization," AIAA SciTech 2019 Forum Proceedings, San Diego, California, January 7-11, 2019.

[14] Allen, L. D., Lim, J. W., Haehnel, R. B. and Dettwiller, I. D., "Rotor Blade Design Framework for Airfoil Shape Optimization with Performance Considerations," AIAA SciTech 2021 Forum Proceedings, Virtual Event, Jan. 2021, DOI:10.2514/6.2021-0068.

[15] Allen, L. D., Lim, J. W., Haehnel, R. B. and Dettwiller, I. D., "Helicopter Rotor Blade Multiple-Section Optimization with Performance Considerations," Vertical Flight Society 77th Annual Forum Proceedings, Virtual Event, May 2021.

[16] Lim, J. W., Allen, L. D., Haehnel, R. B. and Dettwiller, I. D., "An Examination of Aerodynamic and Structural Loads for a Rotor Blade Optimized with Multi-Objective Genetic Algorithm," 77th VFS Annual Forum Proceedings, Virtual Event, May 2021.

[17] Allen, L. D., Lim, J. W., Haehnel, R. B. and Dettwiller, I. D., "Multi-objective Rotor Blade Optimization Framework Advancements," Proceedings of the Vertical Flight Society Aeromechanics for Advanced Vertical Flight Technical Meeting, San Jose, California, Jan. 25-27, 2022.

[18] Eddy, J. and Lewis, K., "Effective Generation of Pareto Sets Using Genetic Programming," Proceedings of the ASME International Design Technical Conferences, Design Automation Conference, Pittsburgh, PA, 2001.

[19] Lim, J. W., "Application of Parametric Airfoil Design for Rotor Performance Improvement," 44th European Rotorcraft Forum Proceedings, Delft, Netherlands, Sep. 2018.

[20] Stellar Science Ltd Co., "Galaxy Simulation Builder (GSB) User Guide, Version 8.1," High Power Electromagnetic Division, Air Force Research Lab, 2019.

[21] Saberi, H., Hasbun, M., Hong, J., Yeo, H. and Ormiston, R. A., "Overview of RCAS Capabilities, Validations, and Rotorcraft Applications," American Helicopter Society 71st Annual Forum Proceedings, Virginia Beach, Virginia, May 2015.

[22] Lim, J. W., "Consideration of structural constraints in passive rotor blade design for improved performance," The Aeronautical

Journal, Vol. 119, No. 1222, December 2015, pp. 1513-1539.

[23] Wenren, Y., Lim, J. W., Allen, L. D., Haehnel, R. B. and Dettwiller, I. D., "Helicopter Rotor Blade Planform Optimization Using Parametric Design and Multi-Objective Genetic Algorithm," 78th VFS Annual Forum Proceedings, Fort Worth, Texas, May 2022.

[24] Tian, S., Tao, F., Du, H., YU, W., Lim, J. W., Haehnel, R., Wenren, Y. and Allen, L., "Structural Design Optimization of Composite Rotor Blades with Strength Considerations," 2022 AIAA SciTech Forum Proceedings, San Diego, CA, January 3-7, 2022.

[25] Rajagopalan, R. G., Baskaran, V., Hollingsworth, A., Lestari, A., Garrick, D., Solis, E., and Hagerty, B., "RotCFD - A Tool for Aerodynamic Interference of Rotors: Validation and Capabilities," American Helicopter Society Future Vertical Lift Aircraft Design Conference Proceedings, San Francisco, California, Jan. 2012.

[26] Sobieczky, H., "Parametric airfoils and wings," *Recent Development of Aerodynamic Design Methodologies*, Springer, 1999, pp. 71-87.

[27] Kulfan, B. M., "Universal Parametric Geometry Representation Method," *Journal of Aircraft*, Vol. 45, No. 1, January-February 2008, pp. 142-158.

[28] Piegl, L, and Tiller, W., "The NURBS Book," *Springer-Verlag*, 2nd edition, 1997.

[29] Pulliam, T. H., "Efficient Solution Methods for the Navier-Stokes Equations," Lecture Notes for the Von Karman Institute for Fluid Dynamics Lecture Series, Brussels, Belgium, Jan. 1986.

[30] Norman, T. R., Shinoda, P., Peterson, R. L. and Datta, A., "Full-Scale Wind Tunnel Test of the UH-60A Airloads Rotor," American Helicopter Society 67th Annual Forum Proceedings, Virginia Beach, Virginia, May 3-5, 2011.

[31] Bousman, W. G., "Rotorcraft Airloads Measurements - Extraordinary Costs, Extraordinary Benefits," NASA TP-2014-218374, August 2014.

[32] McHugh, F. J., "What Are the Lilt and Propulsive Force Limits at High Speed for the Conventional Rotor?," the 34th American Helicopter Society Forum Proceedings, Washington, D. C., May 1978.

[33] Hansford, R. E., "Rotor Load Correlation with the British Experimental Rotor Program Blade," *J. American Helicopter Society*, Vol. 32, No. 3, July 1987.

[34] Perry, F. J., "Aerodynamics of the Helicopter World Speed Record," 43rd American Helicopter Society Annual Forum Proceedings, St. Louis, Mo., May 1987.

[35] Harrison, R., Stacey, S. and Hansford, B., "The Design, Development and Testing of an Advanced Rotor Blade," 64th American Helicopter Society Annual Forum Proceedings, Apr. 29 - May 1, 2008, Montreal, Canada.

[36] Min, B. Y., Klimchenko, V., Gao, A., Dunn, A. F., Matalanis, C. G. and Wake, B. E., "High Speed and Highly Efficient Rotor Blade Design," Vertical Flight Society 78th Annual Forum Proceedings, Fort Worth, Texas, May 2022.